Fracture Analysis of the Debonding between FRP and Concrete using Digital Image Correlation

Mohamad Ali-Ahmad
The Graduate Center of the City University of New York, New York, NY, USA.

Kolluru Subramaniam[*] & Michel Ghosn
The City College of the City University of New York, New York, NY, USA.
*ksubram@ce.ccny.cuny.edu

ABSTRACT: Fiber Reinforced Plastic (FRP) sheets are being used for strengthening existing reinforced and prestressed concrete structures. The effectiveness of the strengthening relies on the load-transfer between the concrete and the FRP. It has been shown that strengthened beams often fail due to shear debonding at the FRP-concrete interface, which results in the delamination of the FRP from the concrete substrate. The failure is caused by a crack, which forms and propagates in a thin layer of concrete beneath the FRP. Results from shear tests performed on concrete blocks strengthened with FRP sheets are presented in this paper. The strain distributions in concrete and FRP were determined using an optical technique known as digital image correlation. The results show that the debonding process can be described in terms of crack propagation through the interface between concrete and FRP. The data provides information to determine the stress versus relative displacement (cohesive fracture behavior) and the fracture parameter G_F (fracture energy).

Keywords: bond; concrete; fiber reinforced plastic; cohesive law; fracture energy; slip.

1. INTRODUCTION

In typical flexural strengthening applications, FRP sheets are bonded to the tension side of the beam to act as external reinforcement. The FRP sheets contribute tensile forces to the internal moment resistance, which results in an increased load carrying capacity of the beam. The stress transfer from concrete to the FRP through the bond generates tensile stresses in the FRP. Thus, the bond between the concrete and the FRP becomes an important factor that controls the level of strengthening achieved. In design applications, the load carrying capacity of a strengthened beam is evaluated considering the rupture mode of failure for the FRP, in addition to the usual modes of failure observed in a typical reinforced concrete beam (Meier et al. 1991, Quantrill et al. 1996, Saadatmanesh & Malek 1998, El-Mihilmy & Tedesco 2000). However, it has been shown that the total strength capacity of the beam is often not attained due to premature failure caused by debonding of the FRP from the concrete substrate (Triantafillou & Pelvris 1990, Lopez Acevedo et al.

2000). To develop rational models for predicting the load response of strengthened beams, the debonding behavior of the FRP from concrete has to be understood. Material models, which consider the debonding mode of failure, can then be developed and incorporated into the analytical/numerical analyses for predicting the load response of strengthened beams.

Many researchers have developed fracture mechanics-based models to predict the theoretical load response for debonding failure of the FRP attached to concrete (Taljsten 1996, Yuan et al. 2001, Wu & Niu 2000). Due to lack of data, these models are based on an assumed cohesive fracture law for the interface. The cohesive crack response is the relationship between the interfacial shear stress and the relative motion (slip) between the concrete and the FRP. Taljsten (1996) developed an approach for predicting the maximum force that the composite layers can resist before debonding by considering energy balance obtained from fracture mechanics. Yuan et al. (2001) studied the influence of the shape of the cohesive law on the load capacity of FRP bonded to concrete. Wu &

Niu (2000) proposed a methodology for predicting the initiation of debonding in reinforced concrete beams using existing material model and compared the debonding load with that obtained from existing experimental data.

Few detailed experimental investigations aimed at determining the strains in the FRP and the concrete during debonding have been conducted (Taljsten 1997, De Lorenzis et al. 2001, Ueda et al. 1999, Bizindavyi & Neale 1999). In these investigations, strains were measured using surface mounted strain gauges. Some researchers have attempted to establish the cohesive law using these data (De Lorenzis et al. 2001, Savoia et al. 2003). The strain obtained from strain gauges, however, does not provide sufficient spatial resolution to allow for an accurate determination of the cohesive stresses. An innovative method for estimating the cohesive law based on numerical inversion of experimental data was developed by Leung & Tung (2001). Nevertheless, direct experimental determination of the cohesive shear stress transfer between concrete and FRP and the cohesive fracture law are currently not available in the literature.

In this paper, the progressive debonding between concrete and FRP is studied using an optical technique known as digital image correlation (DIC). DIC is a high-resolution technique, which provides spatially continuous displacement fields during debonding. From the information provided by DIC, a fundamental understanding of the load versus global slip response of the concrete/FRP interface in terms of observed crack growth is established. A nonlinear cohesive law for fracture along the FRP/concrete interface is developed using the strain obtained from the optical technique.

2. OBJECTIVES

The objectives of this study are: (a) to study the progressive debonding process at the interface between the concrete and the FRP; (b) to determine the stresses transferred between the adherents at different stages of debonding; (c) to develop a fundamental understanding of the load-slip response of the FRP in terms of the crack growth which produces debonding; and (d) to establish the cohesive material law for the interfacial bond between the concrete and the FRP.

3. EXPERIMENTAL TEST SETUP

A test setup was designed to perform direct shear tests on FRP sheets bonded to concrete prisms. The loading arrangement comprised of applying tensile load to the FRP strip, which was attached to the concrete block, while the concrete block was restrained against movement. Concrete blocks of nominal dimensions, length (330 mm), width (125 mm), and height (125 mm) were used. The concrete mix proportion by weight were: 2(coarse aggregates): 2(fine aggregates): 1(cement): 0.45(water). The coarse aggregates comprised of gravel with a maximum size equal to 10 mm while river sand were used as fine aggregates.

The concrete specimens were demolded twenty-four hours after casting and subjected to curing at 99% RH for 28 days. The twenty-eight day compressive strength of concrete, determined using compression cylinders, as per ASTM-C39 (2000), was 38 MPa. The specimens are then placed in the laboratory environment until tested.

Unidirectional carbon fiber reinforced plastic (CFRP) sheets with thickness equal to 0.167 mm, supplied by Mitsubishi Chemical Corporation, were used in this study. The tensile strength and elastic modulus of the FRP sheets in the fiber direction are 3.83 and 230.3 GPa respectively. The FRP sheet was attached in the center on one side of the concrete specimen following the procedures specified by the vendor (Design Guidelines 2000). The width and the bonded length of the FRP sheets were equal to 50 mm and 150 mm respectively. The details of the specimen are shown in Figure 1a.

The loading fixture comprised of a rigid steel I-beam which was anchored to the test machine (Fig. 1c). The concrete specimen was firmly attached to the loading fixture. The load was applied to the FRP sheet while the reaction provided by the steel I-beam restrained the concrete block from movement (Fig. 1b). Two linear variable displacement transformer (LVDT) gauges were attached to the concrete at the edge of the concrete block. The slip between concrete and FRP was determined by measuring the relative displacement between the LVDTs (attached to the concrete) and a thin plate bonded to the FRP surface at the edge of the bonded area. The slip measured using LVDTs is referred to as "global slip" throughout this paper to differentiate it from the slip used in the cohesive law. In all tests, FRP sheets were loaded in tension using a 223-KN capacity hydraulic testing machine (Fig. 1c).
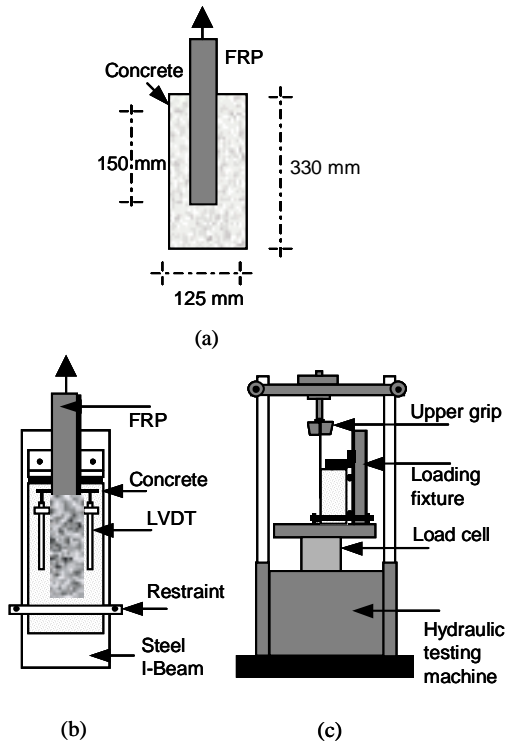
(a)

(b)   (c)

Figure 1. Schematic sketch of the specimen geometry and the loading arrangement: (a) specimen dimensions; (b) loading fixture; (c) test setup.

The tests were performed using global slip as the control variable by increasing it at a constant rate equal to 0.00065 mm/sec up to failure.

4. STRAIN MEASUREMENTS

Surface strains in the FRP and concrete were determined using the Digital Image Correlation (DIC) technique. DIC is a data analysis procedure that uses the mathematical correlation method to analyze digital images of a specimen undergoing deformation. The test setup for DIC comprised of a high-resolution digital camera, which was controlled by a computer (Fig. 2). The specimen was illuminated using normal white light to provide uniform light intensity across the surface.

The surface preparation for the specimen consisted of creating a sprayed-on speckle pattern. The FRP and concrete surfaces were initially sprayed with white paint and then a black mist of paint was applied to create a speckle pattern.
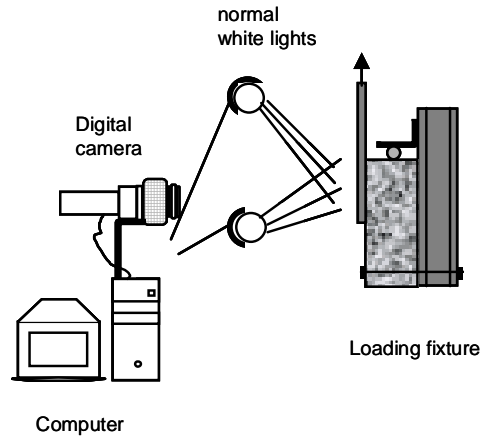

Figure 2. Schematic representation of the digital image correlation test setup.

The correlation, between deformed and the undeformed images, was obtained by tracking the location of each pixel within small neighborhoods called subsets. From the analysis of the digital images, a 2-D displacement field was obtained for all points on the surface.

5. EXPERIMENTAL RESULTS

A typical load versus global slip response is shown in Figure 3. As the global slip is increased, the load response is initially approximately linear up to point A, after which it becomes nonlinear. Point B corresponds to the peak load. There is a slight drop in the load at point B, but the load essentially remains constant with increasing global slip up to failure.
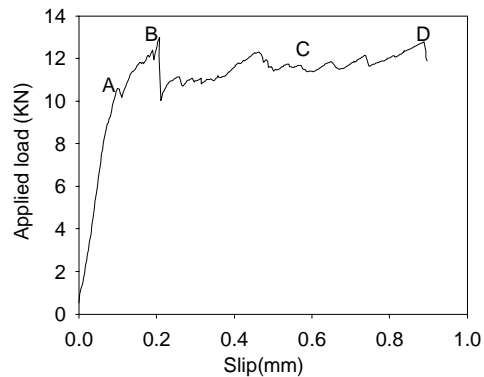

Figure 3. Typical load versus global slip response of the FRP bonded to concrete.

Digital images captured at different stages of loading were used to generate displacement contours on the FRP and the concrete surfaces. The strain distribution was then determined by interpolating the displacement contours using a quintic B-spline collocation method. The strain distributions in the FRP at distinct points of the load response are shown in Figure 4. These contours correspond to the strains in the vertical direction. The contours have varying gray scale intensities; the darker contours indicate higher strains. In Figure 4, the upper edge of the bonded area corresponds to the loaded end of the FRP. From the strain distribution at a typical point between points A & B of the load response (Fig. 4a), the lower portion of the FRP registers approximately zero strain. On moving towards the loaded end, it can be seen that there is a large stress gradient in a small region close to the top. This is typical of any stress riser, like a crack. The strain distribution at point C in the post-peak part of the load response (Fig. 4b) shows that the region of high stress gradient moves further down along the length of the FRP.
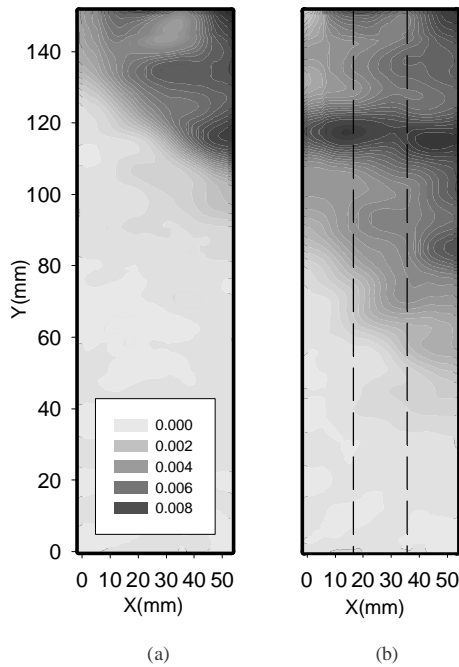

(a)　　　　(b)

Figure 4. Strain contours corresponding to different points of the load-slip response; (a) in the region AB; (b) close to point C.

The measured strains seem to indicate that an interfacial crack initiates in the pre-peak portion of the load response. The analysis of the images captured in the post peak confirmed that there is progressive crack propagation as the relative global slip increases.

6. ANALYSIS OF RESULTS

For the purpose of analysis, the strain variation along the length of the FRP was determined by averaging the strains across the width of a one-inch strip in the center of the FRP sheet (as shown in Figure 4b by the dotted rectangle).

The strain distribution corresponding to the point C of the post-peak part of the load-slip response is plotted in Figure 5. The observed strain distribution along the FRP is essentially equal to zero close to the unloaded end. A rapid increase in strain is observed as we approach the loaded end, following which the value of the strain levels off at approximately 6500με. The observed strain distribution can thus be divided into three main regions: (a) unstressed region; (b) stress transfer zone; and (c) fully-debonded zone. Within the stress transfer zone, the strain distribution is approximately "S" shaped and has a distinctive inflection point in the middle. The strain distribution obtained analytically from linear elastic theory is also plotted in Figure 5 for comparison (Taljsten 1997). It can be seen that the strains predicted by the linear theory approximately coincide with the observed strain initially up to the inflection point. The measured strain deviates significantly from the linear elastic response as we approach the debonded zone. In the debonded zone, the strains are essentially constant and remain unchanged with continuing loading.

The fluctuations of strain observed along the length of the FRP sheet were found to be due to local material variations in the FRP sheet. Optical measurements performed on debonded sheets revealed that the observed local variations correlated well with locations of material inhomogeneities found in the FRP sheet. A local high in the strain distribution was observed at points where fibers were bundled together. Also, variations in the thickness of the FRP sheet and the adhesive were found to contribute to the local variations in strain. The relative pattern of the relative strain distribution caused by these effects however did not change with loading. The

nonlinear strain response in the stress transfer zone produced by shear stress transfer, independent of the local material variations, was approximated by the following expression:

$$\varepsilon(y) = a + \frac{b}{1 + (\frac{y}{c})^h} \qquad (1)$$

where a, b, c, and h were determined using nonlinear-regression analysis of the measured DIC strains.

Figure 6 shows the strain distribution along the FRP (after removing the influence of local material variations) at two different points in the post-peak part of the load-global slip response. It can be seen that as the global slip increases, the length of the fully-debonded zone increases and the stress transfer zone exhibits a lateral shift without stretching towards the unloaded end. It can also be noticed that the size and the shape of the stress transfer zone remains identical in the two cases. The length of the stress transfer zone is constant at approximately 80 mm. Therefore, it can be inferred that the strain distribution in the stress transfer zone corresponding to the post-peak part of the load response is identical.

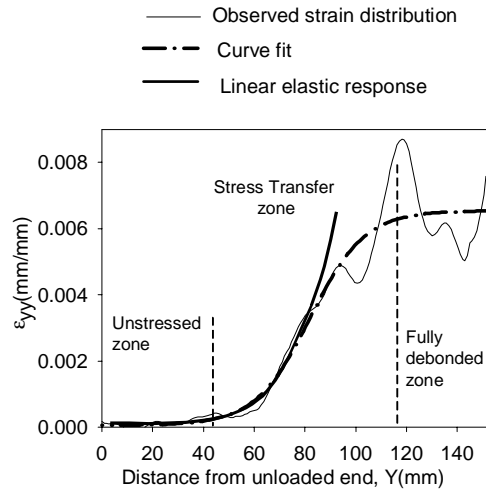The load response of the specimen can now be interpreted in terms of the observed crack growth. Initially, the material response in the linear portion of the load response is linear. As the crack initiates and begins to grow, the load response becomes nonlinear. The peak load is reached when the interfacial crack length becomes equal to a critical value. Subsequently, the crack grows in a self-similar manner at a constant load. As the crack advances, the compliance of the specimen (inverse of the stiffness) increases, which manifests itself in increased global slip. The self-similar crack growth is associated with a characteristic length, which corresponds to the stress transfer zone. As the crack advances, the stress transfer zone, which is similar in shape, moves along the bonded length of the FRP and a longer stretch of the FRP is completely debonded.

The cohesive law for shear fracture at the interface between the FRP and concrete can be determined using the measured strain distribution in the FRP. The cohesive law defines the relationship between the shear stress at the concrete/FRP interface and the relative motion between two points, one located in concrete and the other in the FRP (Figure 7). The following assumptions were made in the analysis:

- The FRP sheets are homogenous and linear elastic.
- The thickness and the width of the FRP sheets are constant along the bonded length.
- The interface is subjected only to shear loading.
- The interface between the FRP and the concrete is assumed to be of infinitesimal thickness.

The interfacial shear stress can be obtained from the measured strain distribution using the following relationship (Taljsten 1997):

$$\tau(y) = t \times E \times \frac{d\varepsilon}{dy} \qquad (2)$$

where $\tau(y)$ = shearing stress distribution along the interface of FRP and concrete; E = elastic modulus of the FRP sheet; t = thickness of the FRP sheet; $\varepsilon(y)$ = strain distribution at the FRP level. From Equation 2, it can be seen that the magnitude of the shear stress depends upon the gradient of the axial strain in the FRP.

The relative slip between FRP and concrete at a given location on the FRP was obtained by integrating the strain along the length up to that point. The concrete substrate was implicitly assumed to be rigid in this analysis. The relationship between the shear stress as calculated

Figure 5. Experimental strain distribution along the FRP sheet corresponding to point C in the post-peak part of the load response.
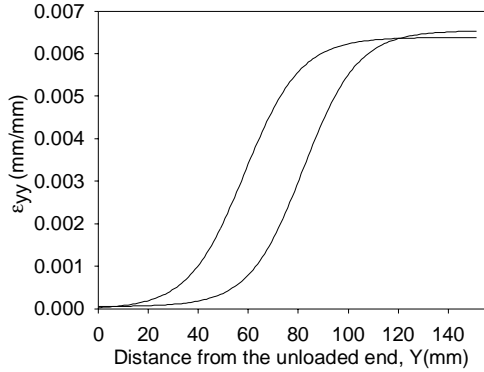
Figure 6. Strain distribution along the FRP sheet corresponding to two different points in the post-peak part of the load-slip response.

using Equation 2 and the relative slip were then obtained. The interfacial material behavior obtained in this manner is known as the cohesive law and is shown in Figure 7. The two continuous curves in Figure 7 correspond to the cohesive law obtained from two different points in the post-peak part of the load response. A close agreement between the cohesive material law determined from two different crack locations corresponding to different points on the load-global slip response is observed. This further confirms the self-similarity of the crack propagation process.

It can be seen that the cohesive law exhibits a softening behavior. It is initially approximately linear up to 40% of the maximum shear stress, after which it is nonlinear up to the peak stress. From the experimental data, the maximum shear stress (τ_{max}) and the corresponding slip (S_o) were determined to be 5.65 MPa and 0.065 mm respectively. After the peak stress, a softening is observed where increas-
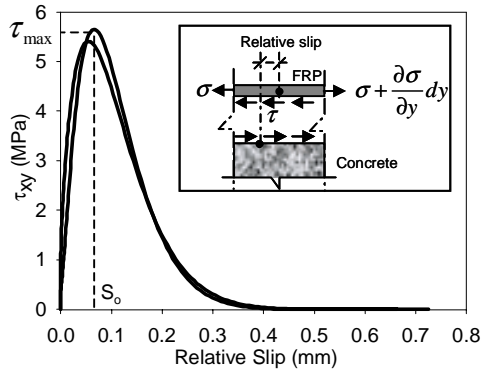

Figure 7. Cohesive crack relationship.

-ing slip results in a decreasing stress. From the material cohesive law, the area under the "τ-s" curve represents the fracture energy G_F. G_F was determined to be 0.82 MPa.mm for interfacial shear fracture between concrete and the FRP.

$$G_F = \int \tau ds \qquad (3)$$

Given that concrete beams strengthened with FRP sheets often fails by debonding between the two materials, the determination of the fracture energy using the method described in this paper provides a method for predicting the effectiveness of strengthening concrete members with FRP sheets.

7. CONCLUSIONS

Based on the results presented in this paper, the following conclusions can be drawn:
1) The progressive debonding of the FRP is produced by a crack which forms and propagates along the interface between the concrete and the FRP;
2) The load versus global slip response of the FRP/concrete bond can be divided into pre and post-peak parts;
3) The observed crack initiates in the pre-peak part of the load response;
4) Once the crack initiates at the interface, it propagates in a self-similar manner at a constant load in the post-peak part of the load response. This steady crack growth is responsible for a constant increase in the global slip of the FRP;
5) In the post-peak part of the load response, where the crack propagates, there is a constant stress transfer length between the concrete and the FRP sheets, which was found to be approximately equal to 80 mm. The stress transfer zone advances along the bonded length of FRP as the crack propagates;
6) The fracture energy, which is required for cracking one unit of area, was found to be constant and independent of the location of the crack along the interface; and
7) Using the digital image correlation allowed for the mapping of the complete strain field which resulted in accurate estimation of the bond fracture strength as represented by the cohesive law and the fracture energy release rate.

REFERENCES

ASTM C-39 (2000). Annual Book of ASTM Standards, Concrete and Aggregates, ASTM.

Bizindavyi, L., & Neale, K.W. (1999). Transfer Lengths and Bond Strengths for Composites Bonded to Concrete. *Journal of Composites for Construction*. Vol. 3, No. 4, pp 153-160.

Chajes, M., Finch, W., Januszka, T., & Thomson, T. (1996). Bond and Force Transfer of Composite Material Plates Bonded to Concrete. *ACI Structural Journal*: Vol.93, No.2, pp. 208-217.

Design Manual (2000). REPLARK SYSTEM. Manufactured by Mitsubishi Chemical Corporation, Japan.

De Lorenzis, L., Miller, B., & Nanni, A. (2001). Bond of Fiber-Reinforced Polymer Laminates to Concrete. *ACI Materials Journal*. Vol. 98, No. 3, pp 256-264.

El-Mihilmy, M.T. & Tedesco, J.W. (2000). Analysis of Reinforced Concrete Beams Strengthened with FRP Laminates. *Journal of Structural Engineering*: Vol.126, No.6, pp. 684-691.

Leung, C.K.Y. & Tung, W.K. (2001). A Three-Parameter Model For Debonding of FRP From Concrete Substrate. *FRP composites in Civil Engineering*: Vol.1, pp. 373-379.

Lopez Acevedo, M. D. M. (2000). Study of the Flexural behavior of Reinforced Concrete Beams strengthened by externally bonded Fiber Reinforced Polymeric (FRP) Laminates. *Doctoral dissertation*. The University of Michigan. 2000.

Meier, U. & Kaiser, H. P. (1991). Strengthening of Structures with CFRP Laminates. *Proceeding of the Conference on Advanced Composites Materials in Civil Engineering*: ASCE, pp. 224-232.

Maeda, T., Asano, Y., Sato, Y., Ueda, T., & Kakuta, Y. (1997). A Study on Bond Mechanism of Carbon Fiber Sheet. *Non-Metallic (FRP) Reinforcement for Concrete Structures*: Vol. 1, Japan Concrete Institute, Japan, pp. 279-286.

Quantrill, R.J., Holloway, L.C., & Thorne, A.M. (1996). Experimental and analytical investigation of FRP strengthened beam response: Part I, II. *Magazine of Concrete Research*, Vol. 48, No. 177, pp. 331-351.

Saadatmanesh, H. & Malek, A.M. (1998). Design Guidelines for Flexural Strengthening of RC Beams and FRP Plates. *Journal of composite for construction*: ASCE, Vol. 2, No. 4, pp. 158-164.

Savoia, M., Ferracuti, B. & Mazzotti, C. (2003). Non-linear bond-slip law for FRP-concrete interface. *FRPRCS-6 Conference Proceedings* (K.H. Tan Ed.), Singapore, 2003, pp. 1-10.

Taljsten, B., (1996). Strengthening of Concrete Prisms using the Plate-Bonding Technique. *International Journal of Fracture*. Vol. 82, pp. 253-266.

Taljsten, B., (1997). Defining Anchor Lengths of Steel and CFRP Plates Bonded to Concrete. *International Journal of Adhesion and Adhesives*, Vol. 17, No. 4, pp. 319-327.

Ueda, T., Sato, Y., & Asano, Y. (1999). Experimental Study on Bond Strength of Continuous Carbon Fiber Sheets. *Proceedings of the FRPRCS-4, SP-188, American Concrete Institute, Farmington Hills, Michigan*. pp. 407-416.

Wu, Z. & Niu, H. (2000). Shear transfer Along FRP-Concrete Interface in Flexural Members. *J. Materials, Conc. Struct., Pavements*: JSCE, No. 662, Vol. 49, November, pp. 231-245.

Yuan, H., Wu, Z., & Yoshizawa, H., (2001). Theoretical Solutions on Interfacial Stress of Externally Bonded Steel/Composite Laminates. *Structural Eng./Earthquake Eng.*, JSCE, Vol. 18, No. 1, pp. 27-39.